


Zero-Frequency Chiral Magnonic Edge States Protected by Nonequilibrium Topology

Pieter M. Gunnink^{1,*}, Joren S. Harms¹, Rembert A. Duine^{1,2} and Alexander Mook³

¹*Institute for Theoretical Physics and Center for Extreme Matter and Emergent Phenomena, Utrecht University, Leuvenlaan 4, 3584 CE Utrecht, The Netherlands*

²*Department of Applied Physics, Eindhoven University of Technology, P.O. Box 513, 5600 MB Eindhoven, The Netherlands*

³*Institute of Physics, Johannes Gutenberg-University Mainz, Staudingerweg 7, Mainz 55128, Germany*

 (Received 16 February 2023; revised 16 May 2023; accepted 22 August 2023; published 22 September 2023)

Topological bosonic excitations must, in contrast to their fermionic counterparts, appear at finite energies. This is a key challenge for magnons, as it prevents straightforward excitation and detection of topologically protected magnonic edge states and their use in magnonic devices. In this Letter, we show that in a nonequilibrium state, in which the magnetization is pointing against the external magnetic field, the topologically protected chiral edge states in a magnon Chern insulator can be lowered to zero frequency, making them directly accessible by existing experimental techniques. We discuss the spin-orbit torque required to stabilize this nonequilibrium state, and show explicitly using numerical Landau-Lifshitz-Gilbert simulations that the edge states can be excited with a microwave field. Finally, we consider a propagating spin wave spectroscopy experiment, and demonstrate that the edge states can be directly detected.

DOI: [10.1103/PhysRevLett.131.126601](https://doi.org/10.1103/PhysRevLett.131.126601)

Introduction.—Over the past decade, it has become clear that the concepts of topological band theory cannot only be applied to electrons [1,2], but also to a whole range of other (quasi)particles, encompassing photons [3,4] and collective bosonic modes in quantum condensed matter systems like phonons [5], plasmons [6,7], and magnons [8]. Among the latter, topological magnon systems, such as magnon Chern insulators [9–16], magnon spin Hall insulators [17–19], magnon Dirac semimetals [20,21], magnon Weyl semimetals [22,23], and higher-order topological magnon insulators [24–26] are especially of interest because they couple to external magnetic fields providing an exceptional handle for control. Arguably, the most fundamental of these phases is the magnon Chern insulator, which supports chiral edge states that could be used as fault-tolerant spin-wave current splitters and interferometers [11,27] and for highly efficient spin transport robust against backscattering at moderate disorder [28,29]. Multiple magnetic materials have been predicted to be magnon Chern insulators from their bulk band structure obtained by inelastic neutron scattering experiments [30–33]. However, the hallmark chiral edge states have to date not been directly observed. Alternatively, as a direct probe of bulk band topology Raman scattering has been proposed [34].

This lack of evidence for chiral bosonic edge states is strongly tied to the fundamental difference between fermion topological insulators and their bosonic analogs. Since bosonic collective excitations do not obey a particle number conservation law, their mathematical description relies on the Bogoliubov-de-Gennes formalism, which comes with a doubled particle space. As a result, the

topologically protected edge states have to appear at finite frequencies above the first bulk band [11,35,36]. For magnon Chern insulators, this means the edge states have energies set by the magnetic exchange energy scale, which is typically meV [31,37]. The corresponding frequency is in the THz range, which is beyond the reach of experimental tools, such as Brillouin light scattering or microwave excitation and detection.

In this Letter, we propose a method to lower the topologically protected chiral edge states in magnon Chern insulators to zero frequency, such that they are easily accessible by microwave techniques. This is achieved by considering magnon excitations on top of a uniform magnetization that is pointing *against* the applied external magnetic field, as opposed to considering excitations on top of a magnetization parallel to the magnetic field, as shown in Figs. 1(a) and 1(b). In such a *nonequilibrium* setup, the magnon excitations decrease the energy of the system, allowing us to tune the frequency of the edge modes to zero frequency. Since the nonequilibrium state is energetically unstable, it has to be rendered dynamically stable, which is achieved by an appropriate spin-orbit torque. Using numerical Landau-Lifshitz-Gilbert simulations we show that the edge modes can be excited at low frequencies, and are topologically protected against backscattering. Finally, we consider a propagating spin-wave spectroscopy (PSWS) experiment with two antennas, and demonstrate that the edge modes can be directly detected at gigahertz frequencies, even in the presence of disorder.

Model.—We consider a two-dimensional magnetic system of localized spins S_i with length S on two sublattices (denoted \mathcal{A} and \mathcal{B}), subject to an external magnetic field \mathbf{H}

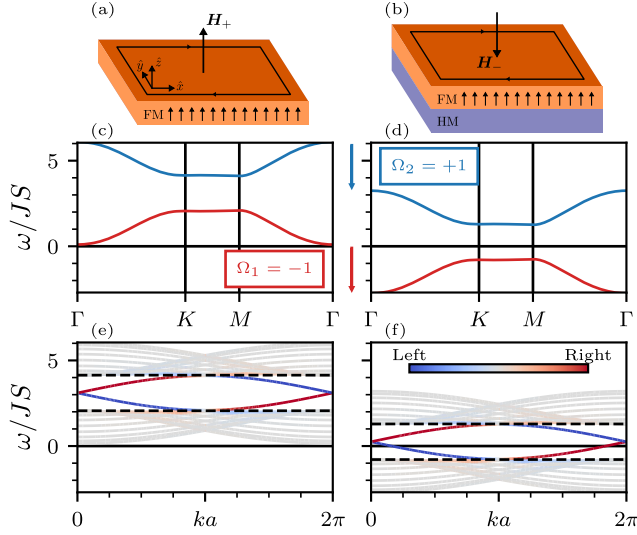


FIG. 1. Strategy for generating zero-frequency chiral magnonic edge states in a magnon Chern insulator FM, comparing the equilibrium (a),(c),(e) with the nonequilibrium (b),(d),(f) situation, with the uniform magnetization (see arrows) and magnetic field \mathbf{H}_{\pm} aligned parallel and antiparallel, respectively. In the nonequilibrium case, the magnetization is stabilized by spin-orbit torques originating from the adjacent HM layer. (c),(d) Bulk magnon band structure with indicated Chern numbers, $\Omega_{1,2}$. (e),(f) Magnon band structure of an armchair edge ribbon. The colorscale of the eigenfrequencies indicates the edge localization, and dashed lines denote the bulk band gap. In equilibrium, $H_{+}/(JS) = 0.1$, the edge states lie at high frequencies, but they are lowered down to zero frequency in nonequilibrium, $H_{-}/(JS) = -2.75$.

with strength H_0 and orientated along the z axis, such that $\mathbf{H} = H_{\pm}\hat{z}$, where we have introduced $H_{\pm} \equiv \pm H_0$. After linearizing the spin Hamiltonian \mathcal{H} in fluctuations around a uniform state we find a two-band spin-wave Hamiltonian. We assume the spin-wave Hamiltonian to realize a magnon Chern insulator, exhibiting topologically nontrivial magnon bands, and topologically protected chiral edge states whose dispersion runs across the bulk band gap. The edge states therefore have a finite energy, which cannot be lower than that of the first bulk band [11,35,36].

The central thesis of this work is that we can use a nonequilibrium state with the magnetization pointing against the external magnetic field to lower the edge states down to zero frequency. We thus consider the state $\mathbf{S}_i = S\hat{z}$, whilst $\mathbf{H} = H_{-}\hat{z}$. We refer to the case of $H = H_{+}$ as the equilibrium, and $H = H_{-}$ as the nonequilibrium. The nonequilibrium state is unstable and will thus relax to the equilibrium state in the presence of dissipation—such as Gilbert damping—with the magnetization parallel to the applied magnetic field. A spin-orbit torque is therefore necessary to render the energetically unstable situation dynamically stable. Experimentally, this could be accomplished by interfacing the ferromagnetic insulator (FM) with a heavy metal (HM), as indicated in Fig. 1(b), such

that the spin Hall effect generates a transverse spin current in the HM, injecting spin into the FM [38].

The spin dynamics are governed by the semiclassical Landau-Lifshitz-Gilbert (LLG) equation

$$\partial_t \mathbf{S}_i = \mathbf{S}_i \times \left(-\frac{\partial \mathcal{H}}{\partial \mathbf{S}_i} + \frac{\alpha}{S} \partial_t \mathbf{S}_i + \frac{J_s}{S} \mathbf{S}_i \times \hat{z} \right), \quad (1)$$

where α is the Gilbert damping, and we allow for the system to be driven by a spin-orbit torque, J_s . We now expand the LLG Eq. (1) in deviations $m_{A/B,i}^{\pm} = (S_{A/B,i}^x \mp iS_{A/B,i}^y)/\sqrt{2S}$ around the uniform state, $\mathbf{S}_{A/B,i} = S\hat{z}$, where $m_{A/B,i}^{\pm}$ refer to excitations for the equilibrium state, $H = H_{+}$, and nonequilibrium state, $H = H_{-}$, on the sublattices A/B . After introducing the Fourier transform of the spin-wave operators, $m_{A/B,i}^{\pm} = \sqrt{2/N} \sum_{\mathbf{k}} e^{i\mathbf{k}\cdot\mathbf{R}_i} m_{A/B,\mathbf{k}}^{\pm}$, the LLG Eq. (1) can be written as a Bogoliubov-de-Gennes (BdG)-like equation in momentum space,

$$i(\tau_0 + i\alpha\tau_z)\partial_t \Psi_{\mathbf{k}}^{\pm} = (\tau_z \mathbf{H}_{\mathbf{k}}^{\pm} + iJ_s\tau_0)\Psi_{\mathbf{k}}^{\pm}, \quad (2)$$

where τ_{η} are the Pauli matrices in particle-hole space and we have introduced the magnon state vector $\Psi_{\mathbf{k}}^{\pm} = (m_{A,\mathbf{k}}^{\pm}, m_{B,\mathbf{k}}^{\pm}, m_{A,-\mathbf{k}}^{\pm*}, m_{B,-\mathbf{k}}^{\pm*})^T$ in particle-hole space.

We first determine the stability criterion for the nonequilibrium state, which can be found by solving the BdG-like Eq. (2) up to zeroth order in \mathbf{k} and up to first order in the dissipative terms, α and J_s . We then find that $\omega_{0,\pm} = H_{\pm} - i(\alpha H_{\pm} - J_s)$. For stability, we require that $\text{Im}[\omega_{0,\pm}] < 0$, which in equilibrium, where $H = H_{+} > 0$, means that the system is stable in the absence of spin-orbit torque. In nonequilibrium, where $H = H_{-} < 0$, we require that $J_s \geq \alpha H$ and thus the nonequilibrium state can be rendered dynamically stable with a sufficiently large spin-orbit torque.

Although our general method is valid for any magnon Chern insulator, we now explicitly consider the well-known magnon Haldane model [14,15], the details of which we review in the Supplemental Material [40]. In the magnon Haldane model, the Dzyaloshinskii-Moriya interaction (DMI) opens the topological gap.

In the absence of dissipation, $\alpha = J_s = 0$, we obtain two sets of two spin-wave solutions to Eq. (2), as a result of the particle-hole symmetry. However, this doubling is not a physical effect and merely the result of the fact that we represent the spin waves using complex scalar fields [43]. We can thus choose to only work with one branch of the solutions, and we then obtain two bands with dispersion relations

$$\omega_{k,1}^{\pm} = H_{\pm} + 3JS + |\mathbf{h}_{\mathbf{k}}|, \quad \omega_{k,2}^{\pm} = H_{\pm} + 3JS - |\mathbf{h}_{\mathbf{k}}|, \quad (3)$$

where J is the exchange constant and $\mathbf{h}_{\mathbf{k}}$ comprises the details of the magnon Haldane model [40]. We show this

bulk dispersion in Figs. 1(c) and 1(d), comparing equilibrium and nonequilibrium. In equilibrium, we obtain only states with positive frequencies, whereas in nonequilibrium, where $H = H_- < 0$, the bands are shifted down in frequency, and we now obtain states with negative frequencies. The negative-frequency modes have opposite handedness compared with the positive frequency modes, and thus rotate counterclockwise, whereas the positive frequency modes rotate clockwise. They also carry opposite angular momentum. The shift down in frequency can be explained from the fact that in nonequilibrium the effective magnetic field $\delta\mathcal{H}/\delta\mathbf{S}_i$ is pointing against the magnetization, thus lowering the frequency of the modes. We refer the reader to a full discussion about the particle-hole symmetry and its implications to the Supplemental Material [40], where we also discuss the stability and band structure in the presence of magnetic anisotropy.

The topological invariant for this system, the Chern number of the band n , is now defined as $2\pi\Omega_n = \sum_{\mathbf{k}} \varepsilon_{ij} \partial_{k_i} \mathcal{A}_j^n$, where $\mathcal{A}_j^n = i \langle \Psi_{\mathbf{k}}^n | \sigma_3 | \partial_{k_j} \Psi_{\mathbf{k}}^n \rangle$ is the Berry connection [11,44,45] and $\Psi_{\mathbf{k}}^n$ is the n th eigenstate. In the bulk band structure, Figs. 1(c) and 1(d), we have indicated the Chern number, ± 1 , for the two bands. In equilibrium, the two bands have opposite Chern number and therefore there are topologically protected chiral edge modes connecting the two bands. In nonequilibrium, the Chern number of the bands is preserved, and since one band is shifted down to negative frequency, we therefore expect the edge modes connecting the two bulk modes to cross zero frequency.

To further illustrate the topological nature of the edge states, we show the band structure of a ribbon, 16 unit cells wide, with armchair edges in Figs. 1(e) and 1(f), and indicate the edge localization in the colorscale. We have chosen compensated boundaries, such that the edge coordination number, i.e., the number of nearest neighbors, is equal to the bulk coordination number, and discuss the case of uncompensated boundaries in the Supplemental Material [40]. In equilibrium, we obtain topologically protected edge states, as can be seen from their localization and their dispersion crossing the bulk band gap, and they thus have a finite frequency. In nonequilibrium the edge states remain, but are lowered in frequency and in fact cross zero frequency. We still have one forward-moving mode localized on one side of the ribbon, and a backward-moving mode on the other side. However, there are forward- and backward-moving edge modes with both positive and negative frequencies, and thus opposite handedness.

Numerical verification of the edge modes.—To verify the existence of the edge states at low frequencies, we numerically solve the LLG Eq. (1), including Gilbert damping and the spin-orbit torque needed to stabilize the nonequilibrium setup. This allows us to capture the full dynamics, in particular nonlinearities that are not included

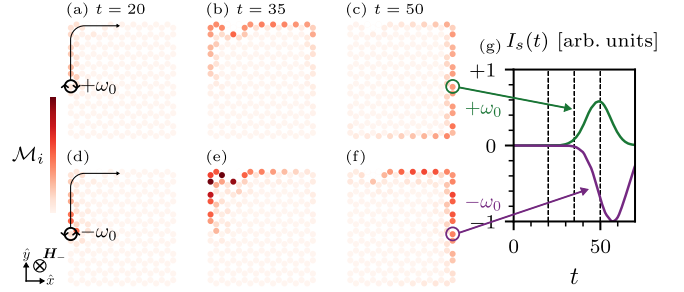


FIG. 2. Spin dynamics simulation of a finite-size system in nonequilibrium, revealing the time evolution under a local excitation pulse with (a)–(c) positive and (d)–(f) negative frequency at $\pm\omega_0$, respectively. The chiral propagation direction of the edge modes is indicated by the arrow. The system starts in a uniform state, $\mathbf{S} = S\hat{z}$, and is continuously excited at one single site at the left edge, circled in (a),(d). (a)–(c) Snapshots of the time evolution of the spin-wave amplitude $\mathcal{M}_i(t)$ for a positive excitation frequency, $+\omega_0$. (d)–(f) Same as (a)–(c) but for a negative excitation frequency, $-\omega_0$. (g) The pumped spin current $I_s(t)$ for a site on the edge. The dashed vertical lines correspond to the times at which the snapshots in (a)–(f) are taken.

in linear spin-wave theory. We describe the specifics of the simulations used in the Supplemental Material [40] and show the resulting dynamics in Fig. 2. We focus on the nonequilibrium dynamics, and use the same parameters used to calculate the band structure in Figs. 1(c) and 1(f), and set $\alpha = 10^{-3}$ and $J_s = \alpha H_-$. A spin wave is excited with positive frequency $\omega_0/JS = 0.7$, Figs. 2(a)–2(c), and negative frequency $\omega_0/JS = -0.7$, Figs. 2(d)–2(f), at one single edge site using a transversely oscillating magnetic field with frequency ω_0 . We show the spin-wave amplitude, defined as the deviation of the spins from the z axis, $\mathcal{M}_i(t) \equiv 1 - S_i^z(t)$.

For both positive and negative excitation frequency, an edge mode is excited, which travels clockwise around the system. Its topological stability due to the absence of backscattering is proven by its bypassing of the defect in the upper left corner, where three edge spins are missing. Importantly, the excitations with opposite frequency have an opposite handedness, i.e., the individual spins rotate in the opposite direction in the (x, y) plane and thus carry opposite angular momentum. This is in sharp contrast to the equilibrium situation, in which all magnons have the same chirality and carry the same angular momentum. Experimentally, this difference could be accessed by means of time-resolved spin pumping [46], because the pumped spin current $I_s(t) \propto \hat{z} \cdot [\mathbf{S}_i(t) \times \dot{\mathbf{S}}_i(t)]$ [47] and the resulting spin-Hall voltage are a direct probe of handedness and, hence, of the topological negative-frequency excitations. To illustrate this, we show the pumped spin current, $I_s(t)$, for a site on the edge in Fig. 2(g). $I_s(t)$ is opposite between positive and negative excitation frequencies, showing that the excitations carry opposite angular momentum. Moreover, the arrival times of opposite excitation

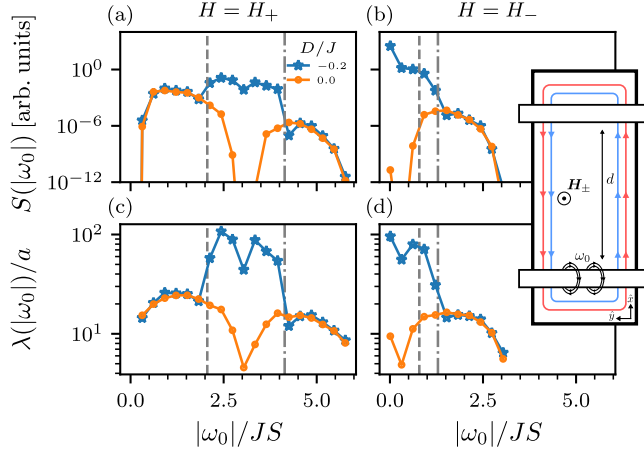


FIG. 3. Propagating spin-wave spectroscopy experiment as sketched in the inset, with edge modes excited by one antenna traveling through the film and picked up by the second antenna. (a),(b) The transmission at finite disorder, $w = 0.05$, and a fixed distance $d = 200a$, as a function of excitation frequency ω , for the equilibrium state ($H = H_+$) and the nonequilibrium state ($H = H_-$) for the topologically trivial state, $D = 0$ and nontrivial state $D/J = -0.2$. Transmission is calculated with a finite Gilbert damping and a stabilizing spin-orbit torque for the nonequilibrium state. (c),(d) The corresponding decay length of the transmission. The dashed and dashed-dotted lines indicate the bottom and top of the bulk band gap.

frequencies differ, which we attribute to the different group velocity of the excited modes. This difference in group velocity can also be seen from the asymmetry of the band structure with respect to $\omega = 0$, Fig. 1(f), and is tuneable by varying the magnetic field. Finally, we observe that the absolute magnitude of $I_s(t)$ is larger for negative-frequency excitations. This is explained by the Gilbert damping, $\alpha\omega$, having the opposite sign for negative-frequency modes compared with their positive frequency counterparts.

Propagating spin-wave spectroscopy.—A central goal in the field of magnon topology is the transport of angular momentum by topologically protected edge states in magnonic devices [48]. Since usual frequencies of the edge states are in the THz range, these cannot be excited using conventional microwave antennas. However, in the nonequilibrium setup, the edge states extend to zero frequency, and are therefore easily accessible. We thus consider a PSWS experiment [49], where two antennas are placed a distance d from each other. One antenna excites spin waves, which are picked up by the second antenna after traveling through the film (see the inset of Fig. 3 for a device illustration). We consider a nanoribbon 10 unit cells wide, with length d , orientated such that the edges are of the armchair type, which corresponds to the dispersion shown in Figs. 1(e) and 1(f).

In the excitation antenna, the Oersted field oscillating with frequency ω excites all possible spin waves with the frequencies $\pm\omega$. Specifically, we model the excitation field by adding a local magnetic field term, $\partial_t \mathbf{S}_i|_{\text{exc}} = \mathbf{S}_i \times \mathbf{h}_i$, to

the LLG Eq. (1), expand in deviations m_i^\pm , and numerically solve the resulting equation of motion to lowest nontrivial order in m_i^\pm in position and frequency space. The second antenna is sensitive to the total microwave power, which we define as the transmission $S(\omega) \equiv \sum_{i \in \mathbb{R}_p} |m_i(\omega)|^2$, where \mathbb{R}_p are the sites connected to the pickup antenna. We also model a concentration w of defects by removing spins, in order to capture the topological protection of the edge modes. The details of this calculation are discussed in the Supplemental Material [40], where we also consider three additional types of disorder to show that the robustness of the zero-frequency edge states is not dependent on the specific disorder considered in the main text.

We show the resulting transmission in Figs. 3(a) and 3(b), comparing the equilibrium and nonequilibrium states, and the topologically trivial state, $D = 0$, and nontrivial state $D/J = -0.2$, where D is the strength of the DMI. We choose $\alpha = 10^{-2}$ and stabilize the nonequilibrium state with a spin-orbit torque, $J_s = \alpha H$. We first focus on the equilibrium state, $H_+/JS = 0.1$, and simulate finite disorder, $w = 0.05$, i.e., 5% of all sites have a defect. In Fig. 3(a), we observe a broad peak in transmission at frequencies in the topologically nontrivial bulk band gap for $D/J = -0.2$. This feature is absent for $D = 0$, proving that it is an effect of the nontrivial topology because the backscattering-immune edge states enable transmission while the bulk state transmission is suppressed.

Turning now to the topologically nontrivial nonequilibrium state, $H_-/JS = -2.75$ and $D/J = -0.2$, where the edge state lies around zero frequency [cf. Fig. 1(f)], we see that transmission instead peaks around zero frequency. Again, we find a clear distinction with the topologically trivial case, $D = 0$, where transmission is suppressed at low frequencies at finite disorder. An important feature of the zero-frequency edge states is their higher transmission compared with the equilibrium edge states. This we attribute to the Gilbert damping, $\alpha\omega$, being proportional to frequency and thus lower for the zero-frequency edge states.

The transmission follows an exponential decay as a function of distance, i.e., $S(d, \omega) \propto \exp[-d/\lambda(\omega)]$, where the decay length $\lambda(\omega)$ is a function of the excitation frequency. We therefore fit the transmission over a range of separation distances $20a < d < 200a$ (a lattice constant) and obtain an estimate for the decay length, $\lambda(\omega)$, which we show as a function of excitation frequency, ω , in Figs. 3(c) and 3(d). We observe that the decay length reflects the topological protection of the edge states, peaking when the edge states are excited. Furthermore, the decay lengths are much larger for $D/J = -0.2$ compared with $D = 0$, reflecting the robustness against disorder of the edge states. Most importantly, in nonequilibrium, in the limit $\omega \rightarrow 0$ the decay length increases, which is in stark contrast to the equilibrium state, where the finite gap induced by the magnetic field blocks transmission.

Discussion and conclusion.—We have shown that by considering the magnetic excitations on top of a non-equilibrium state, stabilized by spin-orbit torques, we can effectively lower the frequency of topologically protected chiral magnon edge modes. We obtain edge states with negative and positive frequency, and we have confirmed their existence by numerically solving the Landau-Lifshitz-Gilbert equation, showing their stability and robustness against defects. Furthermore, we have shown that in a propagating spin-wave spectroscopy experiment, the edge modes can be directly detected.

In the Supplemental Material [40], we provide estimates for the required strength of the external magnetic field and spin-orbit torque for specific material choices. Here we note that in general the magnetic fields and spin-orbit torque, αH_{\perp} , are proportional to the frequency of the edge mode in equilibrium. It would therefore be beneficial to consider this nonequilibrium state in a topological magnon crystal, where the frequencies of the edge modes are set by dipolar interaction, which is in the range of GHz [11,50]. An alternative approach would be to look at the transient regime, by first aligning the system to an external magnetic field, and then reversing the direction of the applied field. For a short transient period one would then observe the same features as discussed here, but after some time the system would relax to equilibrium.

Our strategy can be used to lower other topological magnon excitations to zero frequency. Specifically, magnon Weyl semimetals would be an interesting prospect because zero-frequency Weyl points and associated topological surface states could come with the same transport anomalies as their finite-frequency counterparts [18,51,52]. Beyond magnons, it will be exciting to explore similar ideas for other bosonic Chern insulators, such as those formed by photons [3] or phonons [53,54]. In these bosonic systems, nonequilibrium is accessible through external pumping, analogous to the spin-orbit torque used in this work. Finally, we note that nonequilibrium incoherent Hall-type transport [55–57] could be of interest because low-frequency edge states could potentially dominate transport.

R. A. D. is member of the D-ITP consortium, a program of the Dutch Research Council (NWO) that is funded by the Dutch Ministry of Education, Culture and Science (OCW). This work is in part funded by the Fluid Spintronics research program with Project No. 182.069, financed by the Dutch Research Council (NWO), and by the Deutsche Forschungsgemeinschaft (DFG, German Research Foundation)—Project No. 504261060 (Emmy Noether Programme).

* p.m.gunnink@uu.nl

[1] F. D. M. Haldane, Model for a Quantum Hall Effect without Landau Levels: Condensed-Matter Realization of the “Parity Anomaly,” *Phys. Rev. Lett.* **61**, 2015 (1988).

[2] M. Z. Hasan and C. L. Kane, Colloquium: Topological insulators, *Rev. Mod. Phys.* **82**, 3045 (2010).

[3] F. D. M. Haldane and S. Raghu, Possible Realization of Directional Optical Waveguides in Photonic Crystals with Broken Time-Reversal Symmetry, *Phys. Rev. Lett.* **100**, 013904 (2008).

[4] T. Ozawa, H. M. Price, A. Amo, N. Goldman, M. Hafezi, L. Lu, M. C. Rechtsman, D. Schuster, J. Simon, O. Zilberberg, and I. Carusotto, Topological photonics, *Rev. Mod. Phys.* **91**, 015006 (2019).

[5] G. Ma, M. Xiao, and C. T. Chan, Topological phases in acoustic and mechanical systems, *Nat. Rev. Phys.* **1**, 281 (2019).

[6] D. Jin, L. Lu, Z. Wang, C. Fang, J. D. Joannopoulos, M. Soljačić, L. Fu, and N. X. Fang, Topological magnetoplasmon, *Nat. Commun.* **7**, 13486 (2016).

[7] D. Jin, T. Christensen, M. Soljačić, N. X. Fang, L. Lu, and X. Zhang, Infrared Topological Plasmons in Graphene, *Phys. Rev. Lett.* **118**, 245301 (2017).

[8] P. A. McClarty, Topological magnons: A review, *Annu. Rev. Condens. Matter Phys.* **13**, 171 (2022).

[9] H. Katsura, N. Nagaosa, and P. A. Lee, Theory of the Thermal Hall Effect in Quantum Magnets, *Phys. Rev. Lett.* **104**, 066403 (2010).

[10] K. A. van Hoogdalem, Y. Tserkovnyak, and D. Loss, Magnetic texture-induced thermal Hall effects, *Phys. Rev. B* **87**, 024402 (2013).

[11] R. Shindou, R. Matsumoto, S. Murakami, and J.-i. Ohe, Topological chiral magnonic edge mode in a magnonic crystal, *Phys. Rev. B* **87**, 174427 (2013).

[12] L. Zhang, J. Ren, J.-S. Wang, and B. Li, Topological magnon insulator in insulating ferromagnet, *Phys. Rev. B* **87**, 144101 (2013).

[13] A. Mook, J. Henk, and I. Mertig, Edge states in topological magnon insulators, *Phys. Rev. B* **90**, 024412 (2014).

[14] S. A. Owerre, A first theoretical realization of honeycomb topological magnon insulator, *J. Phys. Condens. Matter* **28**, 386001 (2016).

[15] S. K. Kim, H. Ochoa, R. Zarzuela, and Y. Tserkovnyak, Realization of the Haldane-Kane-Mele Model in a System of Localized Spins, *Phys. Rev. Lett.* **117**, 227201 (2016).

[16] A. Mook, K. Plekhanov, J. Klinovaja, and D. Loss, Interaction-Stabilized Topological Magnon Insulator in Ferromagnets, *Phys. Rev. X* **11**, 021061 (2021).

[17] K. Nakata, S. K. Kim, J. Klinovaja, and D. Loss, Magnonic topological insulators in antiferromagnets, *Phys. Rev. B* **96**, 224414 (2017).

[18] A. Mook, B. Göbel, J. Henk, and I. Mertig, Taking an electron-magnon duality shortcut from electron to magnon transport, *Phys. Rev. B* **97**, 140401(R) (2018).

[19] H. Kondo, Y. Akagi, and H. Katsura, \mathbb{Z}_2 topological invariant for magnon spin Hall systems, *Phys. Rev. B* **99**, 041110(R) (2019).

[20] J. Fransson, A. M. Black-Schaffer, and A. V. Balatsky, Magnon Dirac materials, *Phys. Rev. B* **94**, 075401 (2016).

[21] S. S. Pershoguba, S. Banerjee, J. C. Lashley, J. Park, H. Ågren, G. Aeppli, and A. V. Balatsky, Dirac Magnons in Honeycomb Ferromagnets, *Phys. Rev. X* **8**, 011010 (2018).

[22] F.-Y. Li, Y.-D. Li, Y. B. Kim, L. Balents, Y. Yu, and G. Chen, Weyl magnons in breathing pyrochlore antiferromagnets, *Nat. Commun.* **7**, 12691 (2016).

- [23] A. Mook, J. Henk, and I. Mertig, Tunable Magnon Weyl Points in Ferromagnetic Pyrochlores, *Phys. Rev. Lett.* **117**, 157204 (2016).
- [24] Z. Li, Y. Cao, P. Yan, and X. Wang, Higher-order topological solitonic insulators, *npj Comput. Mater.* **5**, 107 (2019).
- [25] T. Hirose, S. A. Díaz, J. Klinovaja, and D. Loss, Magnonic Quadrupole Topological Insulator in Antiskyrmion Crystals, *Phys. Rev. Lett.* **125**, 207204 (2020).
- [26] A. Mook, S. A. Díaz, J. Klinovaja, and D. Loss, Chiral hinge magnons in second-order topological magnon insulators, *Phys. Rev. B* **104**, 024406 (2021).
- [27] X. S. Wang, H. W. Zhang, and X. R. Wang, Topological Magnonics: A Paradigm for Spin-Wave Manipulation and Device Design, *Phys. Rev. Appl.* **9**, 024029 (2018).
- [28] A. Rückriegel, A. Brataas, and R. A. Duine, Bulk and edge spin transport in topological magnon insulators, *Phys. Rev. B* **97**, 081106(R) (2018).
- [29] X. S. Wang, A. Brataas, and R. E. Troncoso, Bosonic Bott Index and Disorder-Induced Topological Transitions of Magnons, *Phys. Rev. Lett.* **125**, 217202 (2020).
- [30] R. Chisnell, J. S. Helton, D. E. Freedman, D. K. Singh, R. I. Bewley, D. G. Nocera, and Y. S. Lee, Topological Magnon Bands in a Kagome Lattice Ferromagnet, *Phys. Rev. Lett.* **115**, 147201 (2015).
- [31] L. Chen, J.-H. Chung, B. Gao, T. Chen, M. B. Stone, A. I. Kolesnikov, Q. Huang, and P. Dai, Topological Spin Excitations in Honeycomb Ferromagnet CrI_3 , *Phys. Rev. X* **8**, 041028 (2018).
- [32] F. Zhu, L. Zhang, X. Wang, F. J. dos Santos, J. Song, T. Mueller, K. Schmalzl, W. F. Schmidt, A. Ivanov, J. T. Park, J. Xu, J. Ma, S. Lounis, S. Blügel, Y. Mokrousov, Y. Su, and T. Brückel, Topological magnon insulators in two-dimensional Van der Waals ferromagnets CrSiTe_3 and CrGeTe_3 : Toward intrinsic gap-tunability, *Sci. Adv.* **7**, eabi7532 (2021).
- [33] T. Weber, D. M. Fobes, J. Waizner, P. Steffens, G. S. Tucker, M. Böhm, L. Beddrich, C. Franz, H. Gabold, R. Bewley, D. Vonshen, M. Skoulatos, R. Georgii, G. Ehlers, A. Bauer, C. Pfleiderer, P. Böni, M. Janoschek, and M. Garst, Topological magnon band structure of emergent Landau levels in a skyrmion lattice, *Science* **375**, 1025 (2022).
- [34] E. Viñas Boström, T. S. Parvini, J. W. McIver, A. Rubio, S. V. Kusminskiy, and M. A. Sentef, Direct Optical Probe of Magnon Topology in Two-Dimensional Quantum Magnets, *Phys. Rev. Lett.* **130**, 026701 (2023).
- [35] F. Lu and Y.-M. Lu, Magnon band topology in spin-orbital coupled magnets: Classification and application to $\alpha\text{-rui}_3$, *arxiv:1807.05232*.
- [36] Q.-R. Xu, V. P. Flynn, A. Alase, E. Cobanera, L. Viola, and G. Ortiz, Squaring the fermion: The threefold way and the fate of zero modes, *Phys. Rev. B* **102**, 125127 (2020).
- [37] M. Mena, R. S. Perry, T. G. Perring, M. D. Le, S. Guerrero, M. Storni, D. T. Adroja, Ch. Rüegg, and D. F. McMorrow, Spin-Wave Spectrum of the Quantum Ferromagnet on the Pyrochlore Lattice $\text{Lu}_2\text{V}_2\text{O}_7$, *Phys. Rev. Lett.* **113**, 047202 (2014).
- [38] Because of the specific geometry considered here, where the magnetization is perpendicular to the plane, one would need to make use of the anomalous spin Hall effect in a ferromagnetic heavy metal, such as permalloy [39].
- [39] K. S. Das, W. Y. Schoemaker, B. J. van Wees, and I. J. Vera-Marun, Spin injection and detection via the anomalous spin Hall effect of a ferromagnetic metal, *Phys. Rev. B* **96**, 220408(R) (2017).
- [40] See Supplemental Material at <http://link.aps.org/supplemental/10.1103/PhysRevLett.131.126601> for the details of the Haldane model and the effects of anisotropy, a full discussion on the particle-hole symmetry, details on the LLG simulations and transmission calculations, additional sources of disorder, and an estimation of the energy scales. The Supplemental Material contains Refs. [41,42].
- [41] T. Fukui, Y. Hatsugai, and H. Suzuki, Chern numbers in discretized Brillouin zone: Efficient method of computing (spin) Hall conductances, *J. Phys. Soc. Jpn.* **74**, 1674 (2005).
- [42] E. V. Castro, M. P. López-Sancho, and M. A. H. Vozmediano, Anderson localization and topological transition in Chern insulators, *Phys. Rev. B* **92**, 085410 (2015).
- [43] J. S. Harms, H. Y. Yuan, and R. A. Duine, Antimagnonics, *arxiv:2210.16698*.
- [44] M. Lein and K. Sato, Krein-Schrödinger formalism of bosonic Bogoliubov-de Gennes and certain classical systems and their topological classification, *Phys. Rev. B* **100**, 075414 (2019).
- [45] P. M. Gunnink, R. A. Duine, and A. Rückriegel, Theory for electrical detection of the magnon Hall effect induced by dipolar interactions, *Phys. Rev. B* **103**, 214426 (2021).
- [46] A. V. Chumak, A. A. Serga, M. B. Jungfleisch, R. Neb, D. A. Bozhko, V. S. Tiberkevich, and B. Hillebrands, Direct detection of magnon spin transport by the inverse spin Hall effect, *Appl. Phys. Lett.* **100**, 082405 (2012).
- [47] J. Barker and G. E. W. Bauer, Thermal Spin Dynamics of Yttrium Iron Garnet, *Phys. Rev. Lett.* **117**, 217201 (2016).
- [48] A. V. Chumak, V. I. Vasyuchka, A. A. Serga, and B. Hillebrands, Magnon spintronics, *Nat. Phys.* **11**, 453 (2015).
- [49] V. Vlaminck and M. Bailleul, Spin-wave transduction at the submicrometer scale: Experiment and modeling, *Phys. Rev. B* **81**, 014425 (2010).
- [50] R. Shindou, J.-i. Ohe, R. Matsumoto, S. Murakami, and E. Saitoh, Chiral spin-wave edge modes in dipolar magnetic thin films, *Phys. Rev. B* **87**, 174402 (2013).
- [51] Y. Su and X. R. Wang, Chiral anomaly of Weyl magnons in stacked honeycomb ferromagnets, *Phys. Rev. B* **96**, 104437 (2017).
- [52] T. Liu and Z. Shi, Magnon quantum anomalies in Weyl ferromagnets, *Phys. Rev. B* **99**, 214413 (2019).
- [53] Z. Yang, F. Gao, X. Shi, X. Lin, Z. Gao, Y. Chong, and B. Zhang, Topological Acoustics, *Phys. Rev. Lett.* **114**, 114301 (2015).
- [54] P. Wang, L. Lu, and K. Bertoldi, Topological Phononic Crystals with One-Way Elastic Edge Waves, *Phys. Rev. Lett.* **115**, 104302 (2015).
- [55] Y. Onose, T. Ideue, H. Katsura, Y. Shiomi, N. Nagaosa, and Y. Tokura, Observation of the magnon Hall effect, *Science* **329**, 297 (2010).
- [56] S. Murakami and A. Okamoto, Thermal Hall effect of magnons, *J. Phys. Soc. Jpn.* **86**, 011010 (2017).
- [57] A. A. Kovalev and V. Zyuzin, Spin torque and Nernst effects in Dzyaloshinskii-Moriya ferromagnets, *Phys. Rev. B* **93**, 161106(R) (2016).